

This is an Open Access document downloaded from ORCA, Cardiff University's institutional repository: <https://orca.cardiff.ac.uk/id/eprint/102534/>

This is the author's version of a work that was submitted to / accepted for publication.

Citation for final published version:

Gaur, Ruchi, Choubey, Diksha Kumari, Usman, Mohammad, Ward, Benjamin, Roy, Jagat Kumar and Mishra, Lallan 2017. Synthesis, structures, nuclease activity, cytotoxicity, DFT and molecular docking studies of two nitrate bridged homodinuclear (Cu-Cu, Zn-Zn) complexes containing 2,2'-bipyridine and a chalcone derivative. *Journal of Photochemistry and Photobiology B: Biology* 173, pp. 650-660. 10.1016/j.jphotobiol.2017.07.005

Publishers page: <http://dx.doi.org/10.1016/j.jphotobiol.2017.07.005>

Please note:

Changes made as a result of publishing processes such as copy-editing, formatting and page numbers may not be reflected in this version. For the definitive version of this publication, please refer to the published source. You are advised to consult the publisher's version if you wish to cite this paper.

This version is being made available in accordance with publisher policies. See <http://orca.cf.ac.uk/policies.html> for usage policies. Copyright and moral rights for publications made available in ORCA are retained by the copyright holders.



---

# Synthesis, structures, nuclease activity, cytotoxicity, DFT and molecular docking studies of two nitrate bridged homodinuclear (Cu-Cu, Zn-Zn) complexes containing 2,2'-bipyridine and a chalcone derivative

Ruchi Gaur<sup>a</sup>, Diksha Kumari Choubey<sup>b</sup>, Mohammad Usman<sup>c</sup>, Benzamin D. Ward<sup>d</sup>, Jagat Kumar Roy<sup>b</sup>, Lallan Mishra<sup>a</sup>

<sup>a</sup> Department of Chemistry, Institute of Science, Banaras Hindu University, Varanasi 221 005, U.P., India

<sup>b</sup> Department of Zoology, Institute of Science, Banaras Hindu University, Varanasi 221 005, U.P., India

<sup>c</sup> Department of Chemistry, Aligarh Muslim University, Aligarh 202002, U.P., India

<sup>d</sup> Department of Chemistry, University of Cardiff, Cardiff CF10 3AT, UK

---

## ARTICLE INFO

### Keywords:

Dinuclear complex  
X-ray crystallography  
DFT  
DNA cleavage  
Cytotoxicity  
Molecular docking

## ABSTRACT

Nitrate bridged dinuclear complexes of type  $[\text{Cu}_2(\text{L})_2(\text{bpy})_2(\text{NO}_3)](\text{NO}_3)\cdot 4\text{H}_2\text{O}$ , **1** and  $[\text{Zn}_2(\text{L})_2(\text{bpy})_2(\text{NO}_3)](\text{NO}_3)\cdot 4\text{H}_2\text{O}$ , **2** (L = deprotonated form of free ligand LH, [1-(2-hydroxyphenyl)-3-(9-anthracenyl) propenone; bpy = 2,2'-bipyridine] are synthesized and characterized using a battery of physicochemical techniques and X-ray crystallography. A distorted square pyramidal geometry is assigned to them with  $\text{N}_2\text{O}_3$  coordination core around the metal ion. The co-ligand L binds the metal ions through its O,O' atoms in anti-syn mode. The metal centers in complexes **1** and **2** are separated via bridging nitrate group at a distance of 6.073 Å and 5.635 Å respectively. Their structures and absorption spectra are supported by the computational studies using density functional theory (DFT) and TD-DFT. Both complexes exhibit nuclease activity and cleave supercoiled (form I) DNA. The complex **1** preferentially binds major groove of DNA and follows an oxidative pathway whereas complex **2** binds with minor groove of DNA via hydrolytic pathway. Both complexes inhibit topoisomerase I relaxation activity with  $\text{IC}_{50}$  values of 7 and 35  $\mu\text{M}$ . Molecular docking studies support the groove binding and topoisomerase I binding of the complexes. The complex **1** showed a significant cytotoxicity against HeLa cell lines (a cervical cancer cell lines) in vitro with  $\text{IC}_{50}$  value calculated as  $2.9 \pm 0.021 \mu\text{M}$  as compared to  $28.2 \pm 0.044 \mu\text{M}$  for complex **2**. Complex **2** induces the cell apoptosis at a later-stage as compared to complex **1**. The cell apoptosis and topoisomerase inhibition by complexes enable them to be potential candidates as future anticancer drugs.

---

## 1. Introduction

The search for potential anticancer drugs without side effects has always been demanding in drug development processes. In this context, cellular/molecular targets have primarily identified. Recently, the biological action of transition metal complexes are found capable of site specific DNA cleavage and DNA topoisomerase inhibition and elicited considerable interest for diagnostic and anti-cancer chemotherapy [1]. The site specific DNA cleavage by metal complexes is of contemporary interest as these complexes follow either oxidative or hydrolytic DNA cleavage pathways depending on the central metal atom and co-ordinated ligands [2]. In particular, redox inactive metals such as zinc [3] and zirconium [4] prefer hydrolytic cleavage mechanism, whereas redox-active metal centers like iron and copper initiate oxidative

cleavage mechanism owing to the generation of reactive oxygen species (ROS) [5]. Oxidative damage of DNA in the presence of few ternary Cu (II) complexes is attributed to reactive hydroxyl radicals ( $\bullet\text{OH}$ ) generated through site-specific Fenton reactions [6]. Among transition metals, zinc and copper perform various chemical, biological and medicinal roles and are the second and third most abundant metal ions present in the cellular body after iron [7]. Copper homeostasis and metabolism are crucial to various cancerous cells. Moreover, Cu (II) ion can also interact with DNA through intercalation or surface association via N7 guanine residue of DNA [8] and it can significantly propagate reactive oxygen species (ROS) and subsequently induce DNA damage. On the other hand, Zn (II) ion being biologically important [9] and involved in several metalloenzymes, has recently been discovered to play its significant role in tumor suppression [10]. In this context,

---

Corresponding author.

E-mail address: [lmishrabhu@yahoo.co.in](mailto:lmishrabhu@yahoo.co.in) (L. Mishra).

dinuclear and multinuclear complexes are found to possess synergistic effect as compared to their corresponding mononuclear analogues in terms of DNA binding, cleavage, cytotoxicity and their cellular uptake [11,12]. Recently, Spingler et al. reported that dinuclear Cu(II) and Ni

(II) complexes containing 1,3-bis(1,5,9-triazacyclododecyl) propane, change the conformation of right handed B-DNA into left-handed Z-DNA, but their analogous mononuclear complexes could not induce such conformational changes [13]. On the other hand, Khalil et al. described the presence of an oxalating source in dinuclear curcu-min–metal complexes (Zn and Cu). They inhibited the synergistic effect by pre-exhaustion of curcumin reducing potential effect of cytotoxic activity against four cancer cell lines [14]. Thus, the design and synthesis of dinuclear complexes especially of Cu(II) and Zn(II) was found interesting. The tuning to highly efficient anticancer drugs which could regulate metal uptake, trafficking, function and excretion in biological systems and provide better activities in drug resistance cells [15] requires a proper manipulation of both the metal ions and ligand frameworks. A suitable anionic linker or template effects have been successfully exploited as the most effective tools in the direct synthesis of dinuclear complexes. Anions do not function only to balance the charge in metallorganic hybrid species, but they also play a crucial role in creating structural versatility by bridging the components together and provide structures of higher dimensionality and also stabilize their structures. For example, the planar anions such as  $\text{NO}_3^-$  and  $\text{CO}_3^{2-}$  originate supramolecular networks together with cyclic structures [16,17]. The nitrate ligand ( $\text{NO}_3^-$ ), which behaves as monodentate or a bidentate chelating agent [18] particularly shows the  $\mu$ -(O,O')-bridging mode in its copper(II) complexes. On the other hand, nitrate represents very common bridging ligand acting through different coordination modes [19] yet structural and biological studies of metal complexes bridged by nitrate are scarce. Thus, based on such precedence, and in view of remarkable DNA binding, cleavage and cytotoxicity [20,21] exhibited by copper bipyridine complexes planar aromatic organics species such as 2,2'-bipyridine was selected as a ligand. The selectivity of a hydroxyl chalcone embedded with a conjugated anthracenyl frameworks as ligand was also considered important owing to its pharmaceutical importance [22] and ability to act as bidentate O,O' donor which may probably involve in the construction of H-bonded networks in view of our earlier report [23,24]. Thus, in anticipation of some new unprecedented structural frameworks, it was thought worthwhile to condense a chalcone LH (protonated form of L) separately with Cu(bpy) ( $\text{NO}_3$ )<sub>2</sub>·H<sub>2</sub>O and Zn(bpy)( $\text{NO}_3$ )<sub>2</sub>·H<sub>2</sub>O. As expected, such reactions allowed to generate new rare homodinuclear complexes containing Cu (II)-Cu(II) and Zn(II)-Zn(II) metal centers bridged via nitrate groups in each case. We further investigated these nitrate bridged dinuclear complexes for their applications in DNA cleavage studies. The structural tunability of metal complexes was also considered as a beneficial feature to exploit this framework in cytotoxicity and apoptotic studies.

## 2. Experimental Section

### 2.1. Materials and Methods

Dinitrato trihydrate salt of Cu(II) and dinitrato hexahydrate salt of Zinc(II), 2,2'-bipyridine, and 9-anthracenaldehyde were purchased from Sigma Aldrich Chem. Co. and used as received without further purification. The solvents were purchased from E. Merck and were freshly distilled prior to their use. IR (KBr disc, 400–4000  $\text{cm}^{-1}$ ) spectra were recorded on a Varian FTIR 3100 spectrometer; elemental analysis was carried out using Carbo-Erba 1108 elemental analyzer, UV-visible (UV-vis) were recorded on a Jasco V-630 spectrometer. However, <sup>1</sup>H NMR spectra were recorded in DMSO-d<sub>6</sub> using JEOL AL 300 MHz spectrometer and TMS was used as internal reference. ESI-MS measurements were performed by using a Waters Q-TOF Premier mass spectrometer. ESR spectrum of Cu(II) complex was recorded at 273 K and 77 K on a Varian E-line Century Series ESR spectrometer equipped

with a dual cavity and operating at X-band of 100 kHz modulation frequency. Tetracyanoethylene was used as the field marker ( $g = 2.00277$ ).

### 2.2. X-ray Structural Studies

Single crystal X-ray diffraction data of the ligand and complexes were collected in the temperature range of 293(2) K and 150(2) K using an Oxford diffraction XCALIBUR-S CCD area detector diffractometer and graphite monochromatized Mo K $\alpha$  radiation ( $\lambda = 0.71073$ ) from needle shaped crystals in  $\omega$ - $2\theta$  scan mode for all the complexes. Intensities of these reflections were measured periodically to monitor crystal decay. The crystal structures were solved by direct methods and refined by full matrix least squares (SHELX-97) [25]. Due to high degree of hydration, thermal motion and disorder, hydrogen atoms of water of crystallization could not be located. Drawings were carried out using MERCURY [26] and special computations were carried out using PLATON [27]. The precursor complexes of type M(2,2'-bipy) ( $\text{NO}_3$ )<sub>2</sub>·H<sub>2</sub>O (M = Cu(II), Zn(II)) were prepared and characterized using reported procedure [28].

### 2.3. Synthesis of Ligand 1-(2-hydroxyphenyl)-3-(9-anthracenyl)propenone (LH)

The ligand 1-(2-hydroxyphenyl)-3-(9-anthracenyl)propenone (LH) was synthesized by the condensation of 2'-hydroxy acetophenone and 9-anthracenaldehyde in the presence of 50% NaOH solution using a method reported earlier [29]. Yield: 226 mg (70%), M.P. 166 °C, IR (KBr pellet,  $\text{cm}^{-1}$ ): 2924(m)  $\nu$ (C<sub>6</sub>H), 1634(s)  $\nu$ (C=O), 1299(s)  $\nu$ (O<sub>2</sub>H); <sup>1</sup>H NMR (CDCl<sub>3</sub>,  $\delta$  ppm): 12.85(s, 1H, eOH), 6.88–8.93 (m, 13H, Ar), 7.70 (d, 1H, H<sub>d</sub>), 6.91 (d, 1H, H<sub>\beta</sub>), <sup>13</sup>C NMR (CDCl<sub>3</sub>,  $\delta$  ppm): 193.19 (C=O) 163.83 (Ar<sub>6</sub>CO), 142.66 (C- $\alpha$ ), 125.12 (C- $\beta$ ), 118.69, 118.99, 125.48, 126.62, 128.78, 128.98, 129.37, 129.67, 129.75, 129.88, 131.28, 136.64 (eAr), UV-vis (methanol, 10<sup>-4</sup> M):  $\lambda_{\text{max}}$ (nm) ( $\epsilon_{\text{max}} \times 10^4 \text{ M}^{-1} \text{ cm}^{-1}$ ) 251 (3.638), 352(0.7377), 425 (1.0915),  
 $\lambda_{\text{emission}}$  511 nm at  $\lambda_{\text{excitation}}$  424 nm.

### 2.4. Synthesis of Complex [Cu<sub>2</sub>(L)<sub>2</sub>(bpy)<sub>2</sub>(NO<sub>3</sub>)](NO<sub>3</sub>)·4H<sub>2</sub>O 1

A methanolic solution (20 mL) of Cu(bpy)( $\text{NO}_3$ )<sub>2</sub>·H<sub>2</sub>O (0.361 g, 1 mmol) was added drop wise to a solution of LH (0.324 g, 1 mmol) in dichloromethane (5 mL). The reaction mixture was initially stirred for 12 h then refluxed for another 2 h. The resulting solution was then kept in a refrigerator. After 5–6 days, the brown colored needle shaped crystals were obtained. These crystals were washed with diethyl ether and dried in air. Yield: 0.503 g(40%), M.P. > 230 °C, elemental analysis calculated for C<sub>66</sub>H<sub>54</sub>N<sub>6</sub>O<sub>14</sub>Cu<sub>2</sub> (%): C 61.82; H 4.24; N 6.55, Found: C, 61.45; H, 4.68; N, 6.64. ESI-MS: (m/z) calcd.: 1146 found: 1147 [M]<sup>+</sup>. IR (KBr):  $\nu_{\text{max}}/\text{cm}^{-1}$  3436 (OH, H<sub>2</sub>O), 2926(m)  $\nu$ (CH, Ph), 1616  $\nu$ (CO, 2,2'-bpy), and 1382, 1243 $\nu$ ( $\text{NO}_3$ ,  $\mu_{1,3}$ -bridging nitrate). UV-vis. absorptions:  $\lambda_{\text{max}}$  (methanol, 10<sup>-4</sup> M)/nm ( $\epsilon \times 10^{-4}/\text{M}^{-1} \text{ cm}^{-1}$ ) 295 (3.01), 306 (3.08), 454 (2.93) and 657 (0.0389)  $\lambda_{\text{emission}}$ , 526 nm at  $\lambda_{\text{excitation}}$  454 nm.

### 2.5. Synthesis of Complex [Zn<sub>2</sub>(L)<sub>2</sub>(bpy)<sub>2</sub>(NO<sub>3</sub>)](NO<sub>3</sub>)·4H<sub>2</sub>O 2

A solution of Zn(bpy)( $\text{NO}_3$ )<sub>2</sub>·H<sub>2</sub>O (0.363 g, 1 mmol) in methanol (20 mL) was added dropwise to a solution of LH (0.324 g, 1 mmol) in DCM (5 mL) with stirring at room temp. The stirring was further continued up to 12 h then the solution was refluxed for 6 h. After cooling the reaction mixture, methanol (10 mL) was added to it and the solution was stored in a refrigerator. After 5–6 days, the light yellow needle shaped crystals were obtained. These crystals were washed with methanol and dried in air. Yield: 0.435 g (34%), M.P. > 230 °C, elemental analysis calculated for C<sub>66</sub>H<sub>54</sub>N<sub>6</sub>O<sub>14</sub>Zn<sub>2</sub> (%): C, 61.65; H, 4.23; N 6.54, Found: C, 61.98; H, 4.59; N, 6.78. ESI-MS: (m/z) calcd.: 1171 found:

1171 [M + Na-H]<sup>+</sup>. IR (KBr):  $\nu_{\max}/\text{cm}^{-1}$  3446 (OH, H<sub>2</sub>O), 2916(m)  $\nu(\text{CH}, \text{Ph})$ , 1619  $\nu(\text{CO}, 2, 2', \text{bpy})$ , and 1383, 1245  $\nu(\text{NO}_3^-, \mu_{1,3}\text{-bridging nitrate})$ . <sup>1</sup>H NMR: (DMSO-d<sub>6</sub>,  $\delta$  ppm) 8.04–8.32(16H, m, bpy), 7.03–8.71 (m, 26H, Ar), 8.33 (m, 2H, H $\alpha$ ), 6.96 (m, 2H, H $\beta$ ). <sup>13</sup>C NMR: (DMSO-d<sub>6</sub>,  $\delta$  ppm) 168.29 (CJO), 170.87 (ArCO), 143.21 (C- $\alpha$ ), 122.45 (C- $\beta$ ), 149.05, 135.62, 123.42 (bpy), 135.43, 133.07, 132.22, 131.16, 129.12, 128.89, 128.72, 127.45, 126.76, 125.42, 125.67, 125.46, 115.12 (Ar); UV-vis absorptions:  $\lambda_{\max}$  (methanol, 10<sup>-4</sup> M)/nm ( $\epsilon \times 10^{-4}/\text{M}^{-1} \text{cm}^{-1}$ )  $\lambda_{\max}$  250 (2.59), 274 (1.25), 313 (1.27) and 458 (1.29).  $\lambda_{\text{emission}}$ , 538 nm at  $\lambda_{\text{excitation}}$  458 nm.

## 2.6. Electrochemical Studies

Cyclic voltammetry was performed on a CHI 620c electrochemical analyzer. A glassy carbon working electrode, platinum wire auxiliary electrode, and Ag/Ag<sup>+</sup> reference electrode were used in a standard three-electrode configuration. Tetrabutylammoniumperchlorate (TBAP) was used as a supporting electrolyte, and the solution concentration was kept as 10<sup>-3</sup> M.

## 2.7. DNA Cleavage Studies Using Agarose Gel Electrophoresis

In the gel electrophoresis experiments, supercoiled pBR322 DNA was treated separately with metal complexes, and the mixture was incubated for 1 h at 37 °C. The samples were then analyzed by 1% agarose gel electrophoresis [Tris – acetic acid – ethylenediaminetetraacetic acid (EDTA) (TAE) buffer, pH 8.3] for 2 h at 50 V. The gel was stained with 0.5  $\mu\text{g mL}^{-1}$  ethidium bromide, visualized by UV light, and photographed for analysis. The extent of cleavage of form I (SC) DNA was determined by measuring intensities of the bands using a Genosens 1510 Gel Documentation System. The experiments were also monitored on addition of various activators, viz., Na<sub>2</sub>S<sub>2</sub>O<sub>8</sub>, D<sub>2</sub>O (<sup>1</sup>O<sub>2</sub> singlet oxygen trapper), sodium formate, DMSO, KI (•OH radical scavenger), sodium ascorbate (reducing agent) and H<sub>2</sub>O<sub>2</sub> (oxidizing agent).

## 2.8. Topoisomerase Inhibition Assay

DNA topoisomerase I (Topo I) from Escherichia coli was purchased from New England Biolabs, and no further purification was performed. One unit (U) of the enzyme was defined as the amount that completely relaxed 0.5  $\mu\text{g}$  of negatively charged supercoiled pBR322 plasmid DNA in 30 min at 30 °C under standard assay conditions. The reaction mixture (15  $\mu\text{L}$ ) consists of 50 mM potassium acetate, 20 mM Tris-acetate, 10 mM magnesium acetate, 1 mM DTT (dithiothreitol), 0.1 mg/mL BSA, and 1 U of Topo I together with variable concentration of complexes 1 and 2 (0–25  $\mu\text{M}$  and 0–50  $\mu\text{M}$  respectively) and 0.5  $\mu\text{g}$  of pBR322 DNA. The corresponding reaction mixtures were incubated at 37 °C for 1 h, and then they were terminated by the addition of 3  $\mu\text{L}$  of 5 × stock solution of dye consisting of 0.25% bromophenol blue, 4.5% sodium dodecyl sulfate, and 45% glycerol. The electrophoresis of the samples was carried out through 1% agarose in TAE buffer at 50 V for 2 h. The gel was stained with 1  $\mu\text{g mL}^{-1}$  EB and photographed under UV light. The concentration of the inhibitor that prevented 50% of the supercoiled DNA being converted into relaxed DNA (IC<sub>50</sub> values) was calculated from the midpoint concentration of the complex-induced DNA unwinding. To check whether order of addition affected the results, experiments were also carried out in ice, in which the whole reaction mixture was assembled.

## 2.9. Molecular Docking Methodology

The molecular docking is an interactive molecular graphics program to calculate and display feasible docking modes of a pair of protein, enzymes and DNA molecule. The molecular docking studies have been performed by using Autodock Vina version 1.1.2.29 [30,31]. All rotatable bonds within the ligand were allowed to rotate freely and receptor

was considered rigid. The crystal structure of the B-DNA dodecamer d (CGCGAATTCGCG)2 (PDB ID: 1BNA) was retrieved from the protein data bank (<http://www.rcsb.org/pdb>). Visualization of docked systems have been performed using Discovery studio 4.1 and PyMol.30 [32,33].

## 2.10. MTT Assay

HeLa cells were grown in Dulbecco's Modified Eagle's medium (DMEM) supplemented with 10% (vol/vol) FBS and maintained at 37 °C in a humidified atmosphere of 5% CO<sub>2</sub>. The cells (1 × 10<sup>4</sup>) seeded in 96-well plate and grown overnight were treated with different concentration of crude extract at 24 h. Four hours prior to completion of treatment duration, cultures were supplemented with MTT. After incubation at 37 °C, the cells were lysed with dimethyl sulfoxide and absorbance was measured at 570 nm using ELISA plate reader. The percentage of cell viability was calculated using the following formula: Percentage cell viability = (OD of the experiment samples/OD of the control) × 100. IC<sub>50</sub> was calculated by linear interpolation method.

## 2.11. Apoptosis: Acridine-orange/EtBr Staining Protocol for HeLa Cells

The cells (1 × 10<sup>5</sup>) were grown in cover slip and treated with 65  $\mu\text{M}$  of LH, 2  $\mu\text{M}$  of complex 1 and 25  $\mu\text{M}$  of complex 2 for 24 h. Cells were washed in 1 × PBS. Cells were stained with 100  $\mu\text{L}$  of (from stock 100  $\mu\text{g/mL}$ ) of EtBr for 2.5 min and again stained with 20  $\mu\text{L}$  of acridine orange (100  $\mu\text{g/mL}$ ) for 1 min. Cells were washed twice in PBS and suspended in 500  $\mu\text{L}$  PBS. Image was taken from Nikon90i Eclipse fluorescence microscope.

## 3. Result and Discussion

### 3.1. Synthesis and Characterization

Dinuclear complexes 1 and 2 were prepared by the reaction of LH separately with Cu(bpy)(NO<sub>3</sub>)<sub>2</sub>·H<sub>2</sub>O and Zn(bpy)(NO<sub>3</sub>)<sub>2</sub>·H<sub>2</sub>O. The IR spectrum of free LH displayed peaks at 1634 and 1579  $\text{cm}^{-1}$  assigned to  $\nu_{\text{as}}(\text{CJO})$  and  $\nu_{\text{s}}(\text{CJO})$  vibrations respectively. Corresponding peaks were shifted at 1619, 1549  $\text{cm}^{-1}$  and 1617, 1547  $\text{cm}^{-1}$  in the spectra of 1 and 2 respectively. This observation supported the coordination of CJO group of LH to the metal ion. The bands observed at 1382, 1243  $\text{cm}^{-1}$  and 1382, 1245  $\text{cm}^{-1}$  in the spectra of 1 and 2 were assigned to  $\nu_{\text{as}}(\mu_{1,3}\text{-bridging nitrate})$  and  $\nu_{\text{s}}(\mu_{1,3}\text{-bridging nitrate})$  respectively in view of earlier report [34]. No peak for  $\nu_{\text{s}}(\text{OH})$  vibration was observed in the spectra of both complexes. It was therefore, considered that deprotonated OH group of LH had coordinated to the metal ion. The  $\nu(\text{bpy})$  vibration appeared at 1619 and 1623  $\text{cm}^{-1}$  in the spectrum of 1 and 2 respectively. Additional broad band observed at 3436 and 3446  $\text{cm}^{-1}$  in the spectrum of respective complexes was assigned to  $\nu(\text{OH})$  of water molecules.

The <sup>1</sup>H NMR spectrum of complex 2 displayed peaks at  $\delta(\text{ppm})$  8.33 (m, 2H, H $\alpha$ ), 8.04–8.32 (16H, m, bpy), 7.03–8.71 (m, 26H, Ar), 6.96 (m, 2H, H $\beta$ ). Since no peak corresponding to OH proton was observed in the spectrum of the complex 2, it again supported that deprotonated OH group had coordinated with Zn(II) ion. A downfield shift of ethylenic protons could be understood as a consequence of the coordination of neighboring CJO group [35]. The ESI-MS (S1) of complexes recorded in acetonitrile-water showed molecular ion peak at m/z 1147 and 1171 assigned to [M]<sup>+</sup> and [M + Na-H]<sup>+</sup> for complexes 1 and 2 respectively.

### 3.2. Photophysical Properties

The electronic absorption spectra of the complexes and LH recorded in methanol are displayed in Fig. 1(a). The spectrum of LH showed three peaks at  $\lambda_{\max}$  251, 352 and 425 nm. The longer wavelength absorption could be assigned to intramolecular charge transfer (ICT)

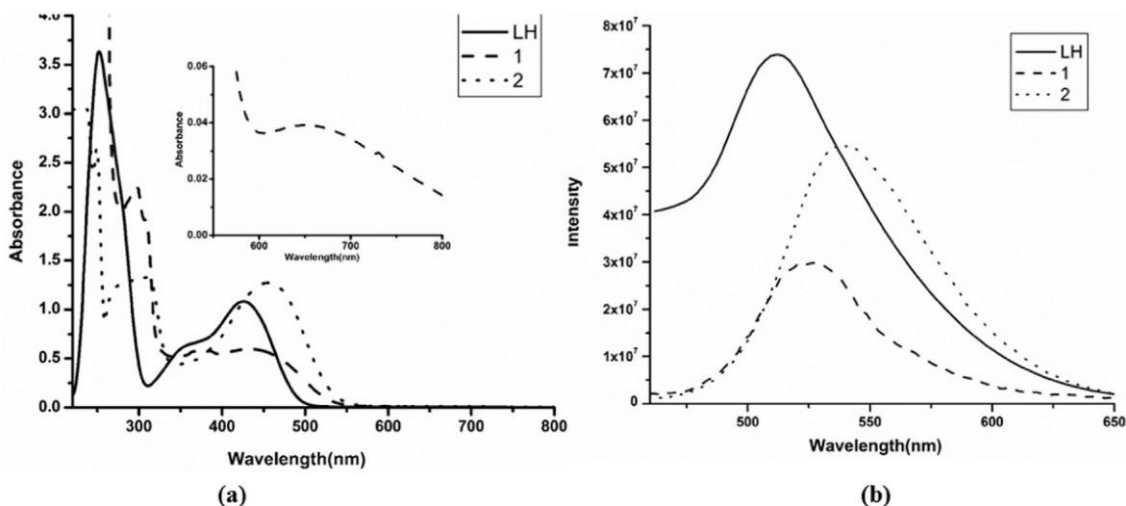


Fig. 1. (a) UV-vis spectra (b) Emission Spectra of LH, Complex 1 and 2 recorded in methanol.

where as high energy peaks originate from  $\pi \rightarrow \pi^*$  transition in con-sistence with earlier report [36]. In the absorption spectrum of complex 1, four peaks displayed at  $\lambda_{\max}$  295, 306, 454 and at 657 nm were as-signed to ligand centered (LC)  $\pi \rightarrow \pi^*$ (bpy), intraligand charge transfer transition (ILCT), O(L)  $\rightarrow$  Cu<sup>II</sup> transition and d-d transitions respec-tively. Normally, a typical square pyramidal complex displays d-d transition band between  $\lambda_{\max}$  550–650 nm [37]. Therefore, a distorted square pyramidal geometry was assigned to complex 1. Absorption spectra of the complexes recorded in methanol at 25 °C for 0–48 h also supported that they are retained in the solution (S2). The complex 2 also displayed similar peaks at  $\lambda_{\max}$  250, 274, 313 and 458 nm. The photophysical properties of substituted chalcones involve mostly asymmetrical donor-acceptor-chalcones and to a minor extent symme-trical donor-acceptor-donor-chalcones in which the acceptor part is the carbonyl group whereas substituted phenyl group serves as donor part [38]. A luminescence peak is observed at  $\lambda_{\text{emission}}$  511 nm from free ligand (LH) on excitation of its solution in methanol ( $10^{-4}$  M) at  $\lambda_{\text{ex}} = 425$  nm and is depicted in Fig. 1(b). The intrinsic probes are usually designed as donor-acceptor substituted  $\pi$ -systems, and their excited-state behavior is usually governed by an intramolecular charge transfer (ICT) process [39]. In view of this report, anthracenyl group present in the chalcone skeleton can act as electron-donor where as its carbonyl group may act as electron-acceptor. Therefore, in present chalcone system, excited state could also be attributed to an in-tramolecular charge transfer process [40] On excitation at  $\lambda_{\text{ex}} = 454$  nm, weak emission from complex 1 was observed at  $\lambda_{\max}$ , 526 nm while complex 2 emitted at 538 nm when excited at  $\lambda_{\text{ex}}$

458 nm. Since, copper (II) complexes do not exhibit emission as Cu(II) ion is well known quencher [41], the weak emission from complex 1 could be assigned to ligand centered emission only. However, sig-nificant emission arising from Zn(II) complex could also be contributed by the emission arising from terminal ligand (bpy). The luminescence from free LH is reduced by ~60% and ~ 26% in its complexes 1 and complex 2 respectively. Emission spectral traces for the complexes in methanol were also recorded at 25 °C for 0–48 h and do not show any significant spectral changes in solution (S3).

### 3.3. Structural Discussion

Since, single crystal X-ray structural analysis of LH is not reported till today therefore its molecular structure is studied and shown in Fig. 2(a). The ligand LH crystallized from dichloromethane: petroleum ether (1:3) provides monoclinic crystal system with a space group P21/ c. The bond length between O(3)eC(017) and O(4)eC(035) was found as 1.245(2) Å and 1.342(2) Å respectively. However, bond length be-tween C(008)eC(023) as 1.405(2) Å was found closer to the value as reported for aromatic ring system [42]. It was observed that CeH and C]O groups are involved in hydrogen bond formation, the motifs C020eH020...O3 and C034eH034...O1 contacts with HeO at a dis-tance of 2.7934 Å and 2.8121 Å respectively. This H-bonded net-work resulted in a supramolecular structure as depicted in Fig. 2(b).

The structures of complexes 1 and 2 were investigated using their X-ray crystallography and data are listed in Table 1. Their molecular structures showed that both metal ions are bridged by a nitrate ion

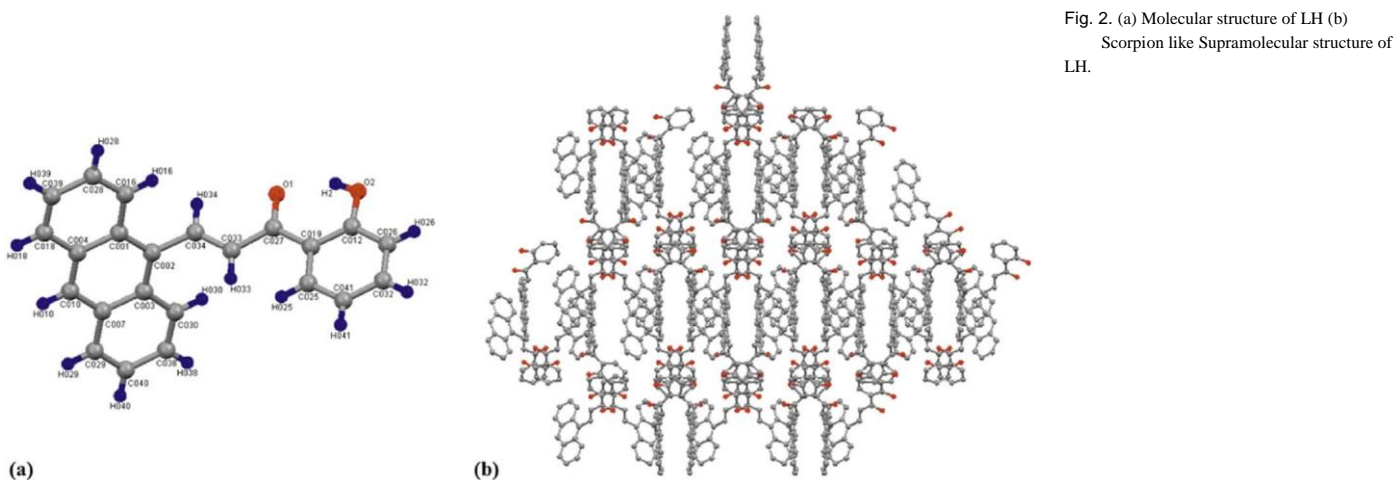


Fig. 2. (a) Molecular structure of LH (b) Scorpion like Supramolecular structure of LH.

**Table 1**  
Data collection and structure refinement parameters for LH, complexes 1 and 2.

Parameters	LH	1	2
Chemical formula	C <sub>23</sub> H <sub>16</sub> O <sub>2</sub>	C <sub>66</sub> H <sub>46</sub> N <sub>6</sub> O <sub>14</sub> Cu <sub>2</sub>	C <sub>66</sub> H <sub>52</sub> N <sub>6</sub> O <sub>14</sub> Zn <sub>2</sub>
Formula weight	324.36	1274.19	1283.92
Temperature	293(2) K	150(2) K	150(2) K
Wavelength (Å)	0.71073	0.71073	0.71073
Crystal system	Monoclinic	Monoclinic	Monoclinic
Space group	P21/c	P121/c1	P121/c1
a(Å)	14.1054(5)	14.5876(6)	13.9836(2)
b(Å)	13.9243(5)	22.9903(9)	23.4802(7)
c(Å)	17.2620(6)	16.9884(5)	17.4585(4)
$\alpha$ (°)	90	90	90
$\beta$ (°)	101.672(4)	96.109(3)	96.988(3)
$\gamma$ (°)	90	90	90
Volume (Å <sup>3</sup> )	3320.3(2)	5665.1(4)	5689.7(2)
Z	8	4	4
Absorption coefficient	0.082	0.828	0.920
F(000)	1392	2616	2648
Theta range for data collection	2.08 to 26.81	3.29 to 25.00°	3.40 to 23.04
Reflections collected/unique	11,914/6531 [R(int) = 0.0196]	42,758/9953 [R(int) = 0.0961]	34,805/7605 [R(int) = 0.0772]
Completeness to theta	98.3%	99.7%	95.6%
Goodness-of-fit on F <sup>2</sup>	1.025	0.916	0.837
Final R indices [I > 2 $\sigma$ (I)]	R1 = 0.0503, wR2 = 0.1187	R1 = 0.0609, wR2 = 0.1608	R1 = 0.0514, wR2 = 0.1228
R indices (all data)	R1 = 0.0952, wR2 = 0.1295	R1 = 0.1217, wR2 = 0.1773	R1 = 0.0913, wR2 = 0.1324

corresponding complexes as depicted in Fig. 3(a) and (b). Although nitrate bears diversified modes of coordination [43] yet nitrate bridged complexes are rare [44]. Bridging of nitrate group as anti-syn bridge-bonding bidentate mode could probably arises from imposition of the bulky anthracenyl group present in the skeleton of the chalcone ligand. The complex 1 crystallized as a monoclinic crystal system with P121/c1 as space group. Its structure consists of a cationic dinuclear molecular unit in which oxygen atoms of nitrate group bridged to two Cu(II) centers. Each Cu(II) ion is penta-coordinated consisting of N<sub>2</sub>O<sub>3</sub> co-ordination core. In view of earlier report [45] a distorted square

pyramidal geometry of complex 1 is supported by  $\tau = 0.183$ , [ $\tau = |\beta - \alpha|/60^\circ$ ] value, where  $\beta$  and  $\alpha$  are the two largest angles around the central atom. The bridging nitrate group is involved in anti-syn bridge-bonding mode with two copper atoms bound to different oxygen atoms of the nitrate ion. The atoms O1, O2, N1 and N2 occupy the basal plane of the square pyramid whereas O3 atom occupies the apical position. The Cu $\cdots$ N and Cu $\cdots$ O distances are found in the reported range S4 [46]. The Cu(II) ions are separated by an intramolecular distance of 6.073 Å (Cu1 $\cdots$ Cu2) and found lower in comparison to earlier reported ni-trato bridged complex most likely owing to the presence of bulky an-thracenyl group present in chalcone moiety [47]. The molecular asso-ciation through non-covalent interaction provides an interesting supramolecular network of helical chains as depicted in S5. Several H-donor and H-acceptor functional groups present in the skeleton of the chalcone form twelve hydrogen bonds S6. The non-conventional hydrogen bonds involve C $\cdots$ H as H-donor and oxygen as H-acceptor. It has a Kitaigorodskii Packing Index (KPI) of 68.9% which shows compact packing with few solvent accessible voids. The structure of complex 1 was also supported by its ESR spectra recorded in solid state as well as in solution (methanol) at room temperature and at liquid N<sub>2</sub> temperature and are shown in [S7].

The coordination environment around Zn(II) was found similar to that of complex 1. The complex 2 was crystallized as monoclinic with space group P121/c1. Each symmetric unit contains [Zn(L)(bpy)] bridged via nitrate anion resulting in a centrosymmetric dinuclear building block along with four co-crystallized water molecules. Each Zn(II) ion is bonded to two N atoms of 2,2' bipyridyl group and two oxygen atoms from L in an anti-syn fashion. The Zn $\cdots$ N (2.086(4) Å) and Zn $\cdots$ O (1.993(3) Å) distances are found similar to that found for re-ported Zn(II) complexes [48]. Both Zn(II) ions are surrounded by a distorted square-pyramidal geometry with  $\tau$  value = 0.133 having C<sub>4v</sub> symmetry. The bpy and chalcone groups are almost perpendicular to the nitrate plane. Two Zn(II) chalcone-bpy units are bridged via a ni-trato group and lie parallel to each other leading to the formation of H-shaped supramolecular structure S8.

Interestingly, two H-shaped supramolecular complexes intersect to each other and form a chair shaped structure Fig. 4(a). There is a two-fold symmetric axis (C<sub>2</sub>) along b direction, leading to chirality within the structure. The intermolecular centroid-centroid distance between two Zn(II) ions are at 5.635 Å. There are twelve non-conventional H-bonds formed in the packing of this complex. The co-crystallized water molecules together with nitrate group are forming a channel like structure as depicted in Fig. 4(b).

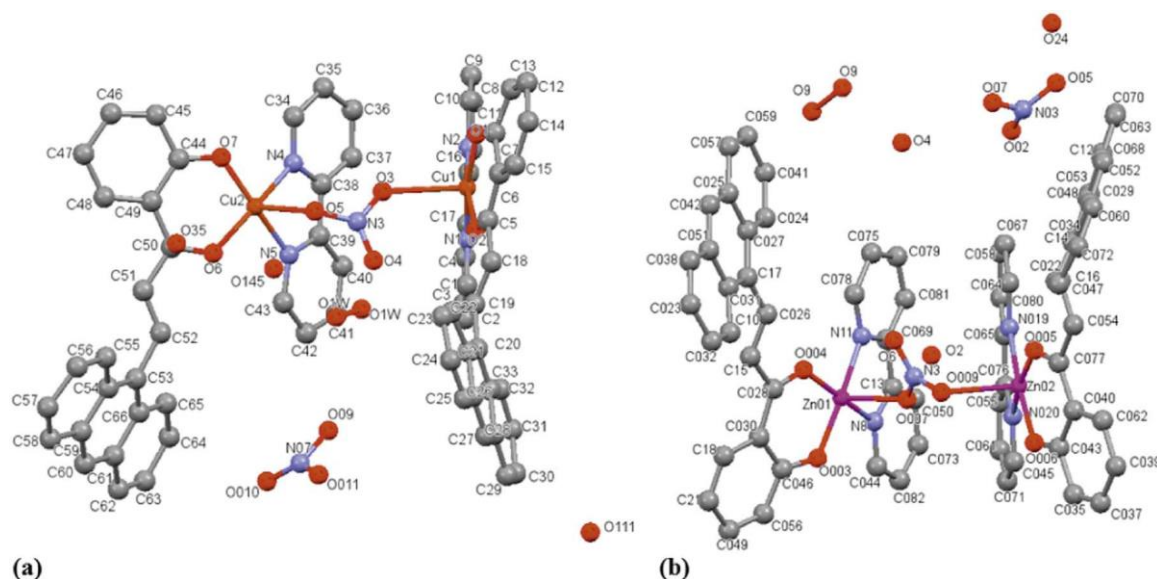


**Fig. 3.** Molecular structure of (a) complex 1, (b) complex 2. Hydrogen atoms are omitted for clarity in complex 1 and 2.

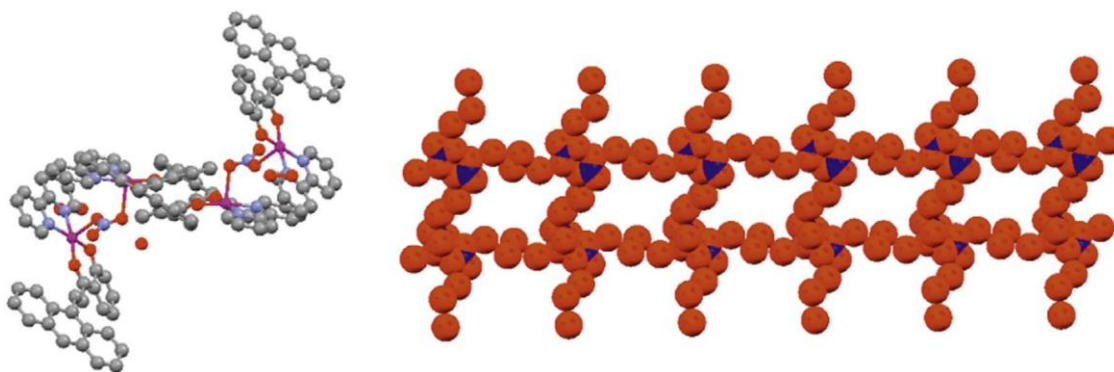


Fig. 4. (a) Chair form structure of complex 2. (b) Channel like structure of complex 2 formed using water and nitrate anion.

Computational data as shown in S9 were calculated using density functional theory (DFT) and TD-DFT and supported the experimentally observed structures and absorption spectra of both complexes.

### 3.4. Cyclic Voltammetry

To understand the redox processes of complex 1, its cyclic voltammetry (S10) was recorded in DMF at 298 K using ferrocene/ferrocenium (Fc/Fc<sup>+</sup>) as an internal standard (0.10 V (80 mv) vs Ag/Ag<sup>+</sup>) in +1 to +2.0 V ranges. Complex 1 showed irreversible reduction and oxidation peaks. The cyclic voltammogram of the complex 1 displayed two cathodic potentials at -0.52 V and -1.33 V which were assigned to the reduction peaks of coordinated L. The bimetallic CuCu complex showed reduction of two Cu(II) ions at 0.85 V and 1.04 V. The oxidation peak observed at 0.85 V is assigned to the oxidation of copper [49].

### 3.5. Interaction of the Complexes With DNA Using DNA Gel Electrophoretic Mobility Assay

For the anticancer drug development, the fine tuning of metal complexes that bind and cleave DNA with structural selectivity has gained interest. The ability of complexes to cleave DNA is usually assessed by agarose gel electrophoresis of supercoiled plasmid DNA under physiological conditions. The gel electrophoretic mobility assay of DNA determines alteration of DNA structure by retardation in migration of supercoiled (Form I) plasmid DNA to nicked circular form (Form II) and to open circular relaxed form (Form III) of DNA using synthetic metal complexes. In order to assess the chemical nuclease activity, pBR322 DNA was incubated with varying concentrations of complexes 1 and 2 (0–50  $\mu\text{M}$ ) separately in tris buffer for 1 h. The mobility graphs are shown in Figs. 5(a and b) and 6(a and b). The complex 1 converts > 50% of form I into form II at a concentration of 30  $\mu\text{M}$ , whereas, for a similar level of conversion, ~35  $\mu\text{M}$  of complex 2 was required. It suggested that Cu(II) complex 1 significantly cleaved DNA as compared to that of Zn(II) complex.

### 3.6. DNA Cleavage in Presence of Groove Binders

In order to identify the potential interacting site of the complexes with supercoiled plasmid pBR322 DNA, gel electrophoretic mobility assay was performed in presence of both minor groove binding agent 4',6-diamidino-2-phenylindole (DAPI) and major groove binding agent, methyl green (MG). The supercoiled DNA was treated with DAPI and MG prior to the addition of complexes 1 and 2 even in lower concentration (20  $\mu\text{M}$ ). As depicted in Fig. 7 in presence of complex 1 and MG, form I DNA is completely converted in form II and form III DNA. However, form I DNA is completely converted in form II and form III DNA in presence of complex 2 together with DAPI. This experiment supported that complex 1 has a tendency of binding with the major groove of DNA whereas complex 2 prefers minor groove of DNA.

### 3.7. Investigation of DNA Cleavage in Presence of Activator and Radical Scavengers

The nuclease mechanism could be inferred by monitoring the quenching of DNA cleavage in the presence of various radical scavengers such as singlet oxygen trapper (NaN<sub>3</sub>, D<sub>2</sub>O), both oxidizing and reducing agent (H<sub>2</sub>O<sub>2</sub>), •OH radical scavenger (sodium formate, KI, DMSO) and reducing agent (sodium ascorbate). Complex 1 in the presence of sodium formate and DMSO as a hydroxyl radical scavenger and sodium ascorbate as reducing agent did not cleave efficiently under identical conditions as depicted in S11. The possibility of singlet oxygen (<sup>1</sup>O<sub>2</sub>) pathway was discarded owing to cleavage of DNA in the presence of activator NaN<sub>3</sub> and also in D<sub>2</sub>O (singlet oxygen trapper). The complex 1, in the presence of H<sub>2</sub>O<sub>2</sub> converted from I form to II form of DNA even at lower concentration (20  $\mu\text{M}$ ). Therefore, DNA cleavage promoted by the complex 1 might occur via an oxidative pathway [20]. No evident inhibition of DNA cleavage by complex 2 was observed in the presence of scavengers such as NaN<sub>3</sub>, D<sub>2</sub>O and H<sub>2</sub>O<sub>2</sub> which suggested that DNA cleavage promoted by it follows neither singlet oxygen (<sup>1</sup>O<sub>2</sub>) pathway nor oxidative pathway “see Fig. S12 in Supplementary

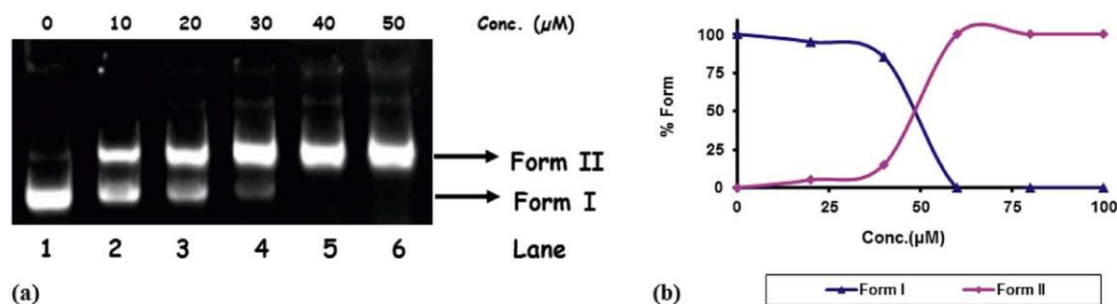


Fig. 5. Ethidium bromide stained agarose gel (1%) of pBR322 plasmid DNA (300 ng  $\mu\text{L}^{-1}$ ) in the presence of complex 1 after 1 h of incubation: lane 1, DNA control; lane 2, pBR322 + 10  $\mu\text{M}$ ; lane 3, pBR322 + 20  $\mu\text{M}$ ; lane 4, pBR322 + 30  $\mu\text{M}$ ; lane 5, pBR322 + 40  $\mu\text{M}$ ; Lane 6, pBR322 + 50  $\mu\text{M}$  (b) Cleavage of supercoiled pBR322 DNA showing the decrease in Form I DNA and the formation of Form II DNA with increasing concentration of complex 1.

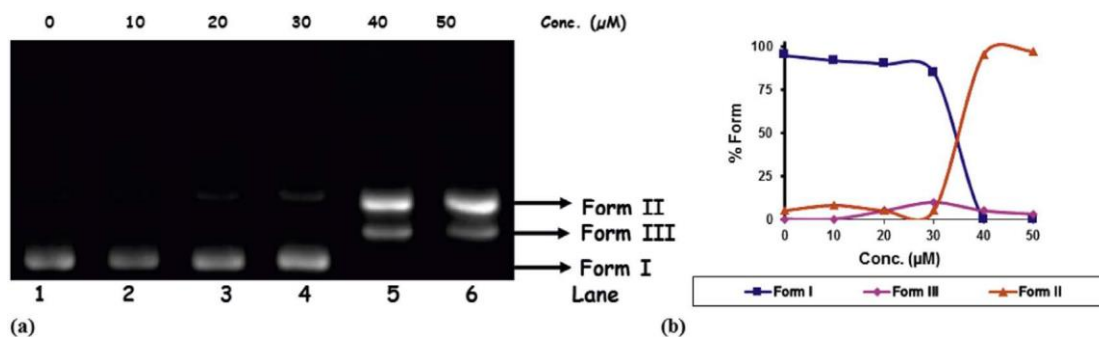


Fig. 6. Ethidium bromide stained agarose gel (1%) of pBR322 plasmid DNA ( $300 \text{ ng } \mu\text{L}^{-1}$ ) in the presence of complex 2 after 1 h of incubation: lane 1, DNA control; lane 2, pBR322 +  $10 \text{ } \mu\text{M}$ ; lane 3, pBR322 +  $20 \text{ } \mu\text{M}$ ; lane 4, pBR322 +  $30 \text{ } \mu\text{M}$ ; lane 5, pBR322 +  $40 \text{ } \mu\text{M}$ ; Lane 6, pBR322 +  $50 \text{ } \mu\text{M}$  (b) Cleavage of supercoiled pBR322 DNA showing the decrease in Form I DNA and the formation of Form II DNA with increasing concentration of complex 2.

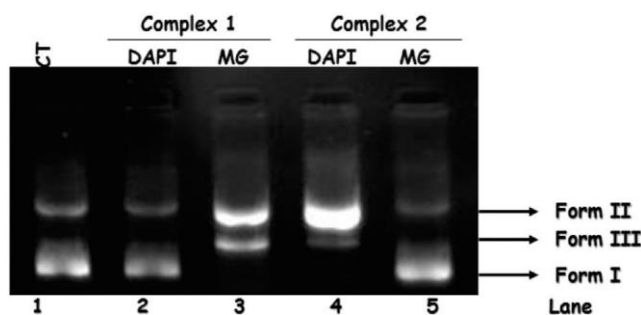


Fig. 7. Agarose gel electrophoresis pattern of pBR322 plasmid DNA (300 ng) by the complexes ( $20 \text{ } \mu\text{M}$ ). Lane 1, DNA control; Lane 2, DNA + complex 1 + DAPI; Lane 3, DNA + complex 1 + methyl green; Lane 4, DNA + complex 2 + DAPI; Lane 5, DNA + complex 2 + methyl green.

material<sup>9</sup>. There are several reports that dinuclear metal ion sites may hydrolyze phosphate esters and RNA by double Lewis acid activation with one metal ion binding to the incoming nucleophile, the second metal ion binding to the leaving group, and both metal ions binding to the phosphodiester [50]. The complex also showed similar kind of hydrolytic mechanism as observed in crowded phenolate type complexes such as quercetin zinc(II) complex [51]. So, it is concluded that complex 2 might be following a hydrolytic pathway.

### 3.8. Topo I Inhibition Assay

In cancer therapeutics, several new targets such as enzymes and proteins are constantly involved in critical cellular processes including DNA replication and cell division. DNA topoisomerase I (topo I) is a protein that catalyzes topological problems as well as nuclear processes such as DNA replication, transcription, repair and chromatin by unwinding duplex DNA [52]. Topoisomerase (topo I) cleaves one strand of supercoiled plasmid DNA pBR322 as well as a phosphodiester bond to the resultant unwound relaxed DNA [53]. In physiological conditions, the DNA cleavage and ligation reactions catalyzed by the topoisomerase I are tightly coordinated and produce rarely detected covalent 3'-

phosphotyrosyl adduct intermediate [54]. Numerous drugs like irinotecan, topotecan and camptothecin (CPT) can inhibit topoisomerase I by blocking the religation step and enhancing the formation of persistent DNA breaks responsible for cell death [35]. The effect of complexes 1 and 2 on the activity of Topo I was investigated on plasmid DNA pBR322 cleavage assay by agarose gel electrophoresis. The investigation shows that complexes 1 and 2 inhibit topoisomerase I in a concentration dependent manner. Topoisomerase inhibition assay anticipates a direct determination of the drug's effect on the unwinding of a supercoiled duplex DNA to a nicked open circular and relaxed DNA. As shown in Fig. 8(a) and (b), the supercoiled DNA pBR322 was fully relaxed by the topo in the absence of complexes 1 and 2 (lane 2). However, on increasing the concentration of complex 1 ( $0-25 \text{ } \mu\text{M}$ ) and 2 ( $0-50 \text{ } \mu\text{M}$ ) respectively, the relaxed DNA (form II) was inhibited (lanes 3-7). Complex 1 completely inhibited Topo I and similar results were also observed with complex 2. The  $\text{IC}_{50}$  values for complexes 1 and 2 were found to be  $7$  and  $35 \text{ } \mu\text{M}$  respectively. Recently, it has been reported that dinuclear copper(II) complex showed inhibitory effects on the catalytic activity of topoisomerase I at a concentration,  $\sim 12.5 \text{ } \mu\text{M}$  [55]. The complexes 1 and 2 were found to be a better candidate in the inhibition of topoisomerase I as compared to some of the standard topoisomerase I inhibitors like camptothecin, doxorubicin, novobiocin, etoposide [56].

### 3.9. Molecular Docking With DNA

The orientation of molecules can direct the recognition of precise sequences and structures of nucleic acids which plays a prominent role in the field of metallo pharmaceutical. The molecular docking studies have a noteworthy feature in demonstrating the drug-DNA interaction in the rational designing of drugs as well as enlighten the mechanistic insight study by inserting a small molecule towards the binding affinity site of the DNA primarily in a non-covalent fashion which can easily envisage the interactions between the nucleic acids of DNA and the drug molecules. The conformation of docked complex usually assesses in terms of hydrogen bonding, energy and hydrophobic interaction between the DNA and complex.

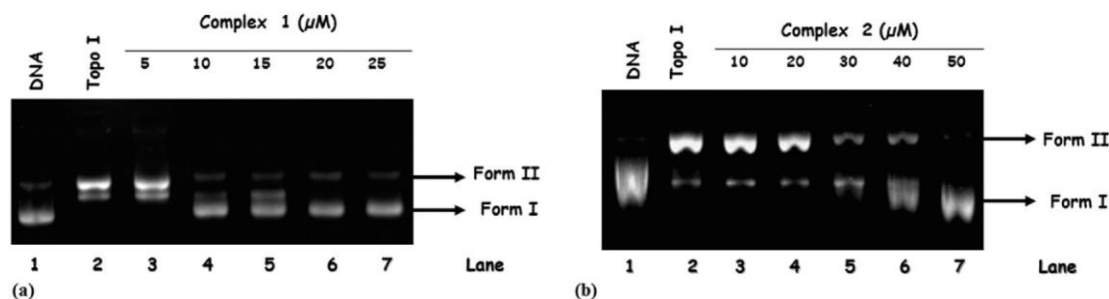


Fig. 8. Effects of different concentrations of 1 and 2 on the activity of DNA Topoisomerase I.

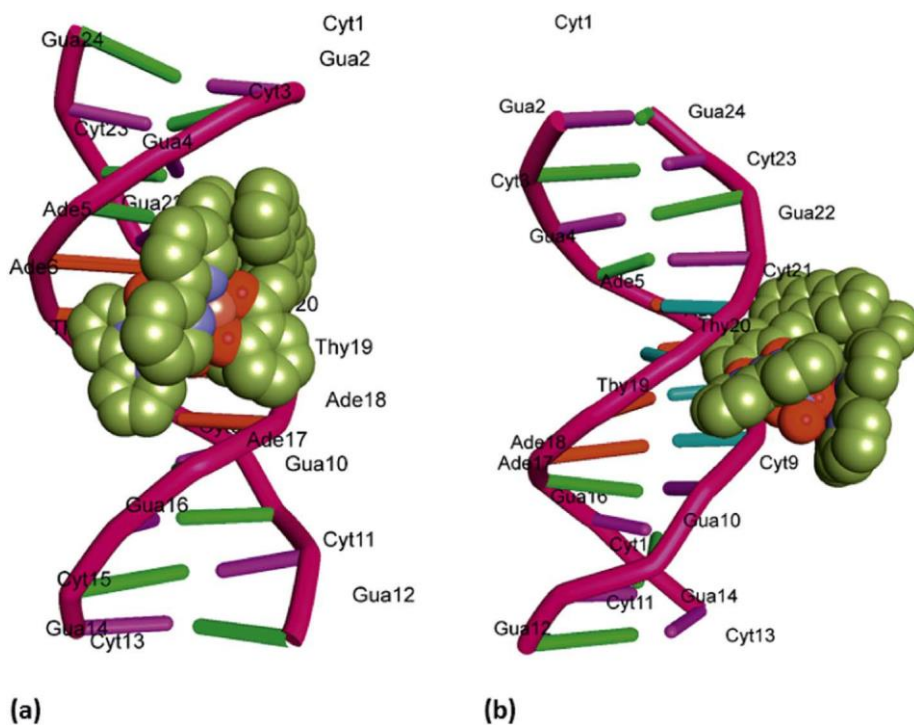


Fig. 9. Representative docking structure of groove binding of the DNA with complexes 1(a) and 2 (b).

The energetically favorable docked pose attained from the rigid molecular docking of complexes 1 and 2 with a DNA duplex of sequence d(CGCGAATTCGCG)2 dodecamer (PDB ID: 1BNA) was executed in order to foresee the binding mode along with the most minimum energy favored orientation (Fig. 9). The result shows that complex 2 interacts with the minor groove of DNA via electrostatic/hydrophobic interactions as illustrated in S13. The outcome binding energy of docked ligand and complex 1 with DNA was found to be  $-6.4$  and  $-8.6$  kcal/mol, respectively indicating strong binding propensity towards the minor groove of DNA. While complex 1 favored major groove binding propensity dominated by electrostatic non covalent interaction with binding energy  $-8.3$  kcal/mol. All the docking results are correlating well with the experimental binding and cleavage studies with DNA.

### 3.10. Molecular Docking With Human Topoisomerase I

In order to determine the mechanistic basis for the inhibitory action and to obtain accurate binding mode on Topo I, the complexes 1 and 2 were studied. The resulting docked models exhibited a dual mode of binding on Topo I due to conformation changes (viz, structural

flexibility) of the interacting complexes 1 and 2. Fig. 10 shows aromatic rings of complexes approaching the DNA cleavage site in the Topo I–DNA complex and forming a stable complex through  $\pi$ – $\pi$  stacking interactions between the purine and pyrimidine ring in the minor groove on the scissile strand and C112 and A113 on the non-scissile strand, parallel to the plane of base pairs. The aromatic (anthracene and bi-pyridine) chromophore fragments of the complexes also successfully forms various hydrophobic contacts like  $\pi$ – $\pi$  Stacked,  $\pi$ -Alkyl, and  $\pi$ -Sulfur to the various amino acids of the Topo I enzyme, particularly Leu 721, Lys 436 and Lys 721 which is considered an essential amino acid that interacts with the ligand in the DNA–Topo I active site. Additionally, aromatic rings facing perpendicularly to the plane of base pairs which strongly block the rewinding step of the phosphoester. Furthermore, DNA-intercalating forces were much more important for the ligand to the surrounding amino acids residues of the protein, or to the base pairs. Our molecular docking study proved the importance of DNA intercalating ability of 1 and 2 as well as  $\pi$ -alkyl and  $\pi$ - $\pi$  stacking hydrophobic interaction with the enzyme in the cleavage site as non-covalent interaction are listed in S13. This result suggests that blocking the religation of the G11 hydroxyl group could be the main design point

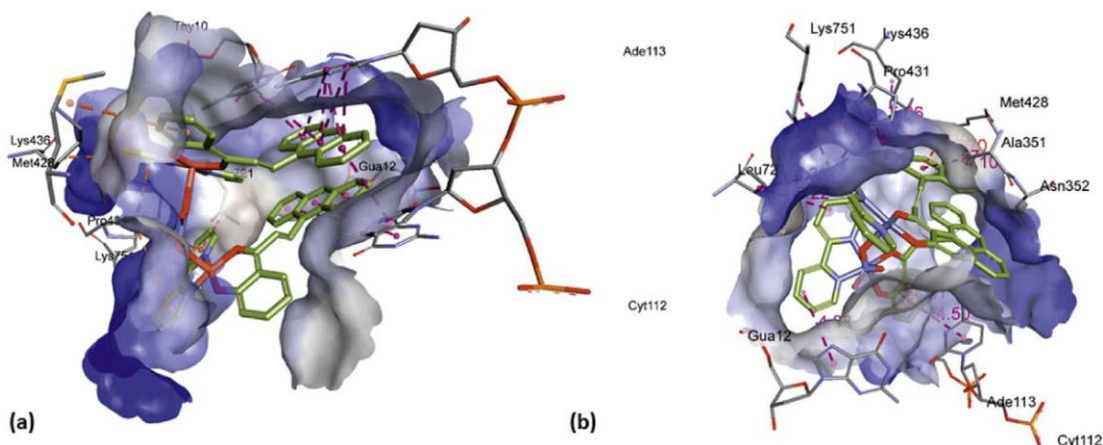


Fig. 10. Representative structure of the most populated cluster for the topoisomerase I-DNA-complexes 1(a) and 2 (b) docking.

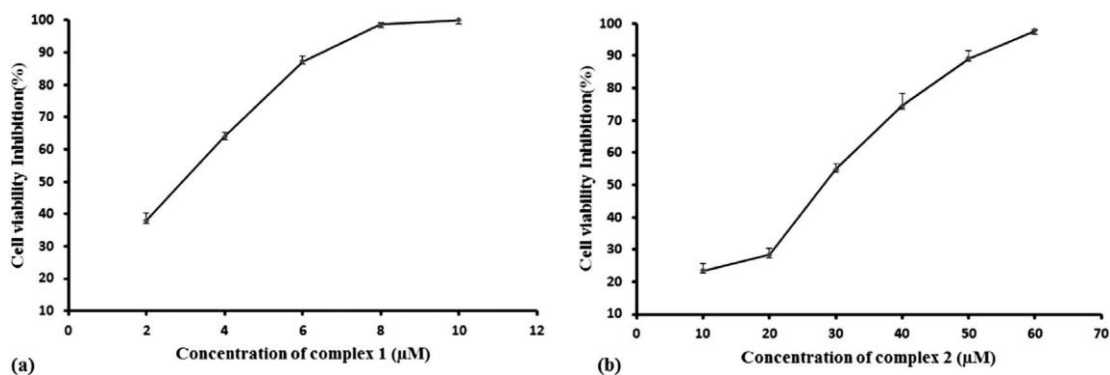


Fig. 11. Cytotoxicity profile of complex 1 and 2 at different concentrations, inhibitory concentration of complex 1 and 2 at which 50% of HeLa cells died is calculated to be  $2.9 \pm 2.13$  and  $28.2 \pm 4.47$   $\mu\text{M}$  respectively.

for novel Topo I inhibitors. The resulting binding affinity of minimum energy-docked structure was found to be  $-16.0$  and  $-14.3$  kcal/mol respectively, revealing the potent greater binding affinity between Human–DNA–Topo I and complex 1 as compared to complex 2. The model studies is suggestive of potential basis for conceivable design of novel anticancer drugs targeting active site of Topo I.

### 3.11. Cytotoxic Study

Cell toxicity is a common limitation in terms of development of new compounds into the chemotherapeutic pharmaceutical industry. Therefore, in this study we were motivated to check the cytotoxicity potential of newly synthesized complexes against human cervical car-cinoma cancer cells. The cell toxicity was commonly measured by MTT assay technique as a reliable method to determine bioactivity of the compounds. The transformation of 3-(4,5-Dimethylthiazol-2-yl)-2,5-diphenyltetrazolium bromide (MTT) to formazan by mitochondrial dehydrogenases serves as an indicator of cell viability [57]. A decrease in formazan production indicates a reduction in the number of meta-bolically active cells i.e. decrease in cell viability. MTT assay was done to test the ability of complexes 1 and 2 to inhibit cell growth and induce cell death in a HeLa (human cervical carcinoma) cancer cell lines as it constitute a highly proliferative human cancer model. The complexes 1 and 2 and LH showed reduction in the viability of the HeLa cells in a concentration dependent manner at 24 h which reflects its significant potency as growth inhibitor and it is shown in Fig. 11 and S14. The half maximal inhibitory concentration ( $\text{IC}_{50}$ ) values of complex 1 ( $2.9 \pm 0.021$   $\mu\text{M}$ ), is lower than that of complex 2 ( $28.2 \pm 0.044$   $\mu\text{M}$ ) and its ligand LH ( $71.0 \pm 0.043$   $\mu\text{M}$ ). It is noteworthy that complex 1 has a better  $\text{IC}_{50}$  value than complex 2 in topoisomerase inhibition study. As compared to cisplatin, as well as some recently reported copper and zinc complexes, the  $\text{IC}_{50}$  value of complex 1 against HeLa cells suggests a stronger cytotoxic action of this complex

than that of cisplatin and other complexes [58,59]. Both complexes showed potential cytotoxicity as compared to recently reported copper and zinc complexes of aminonaphthoquinone derivative [60]. Thus, complex 1 turned out to be a potential cytotoxic complex which war-rants a deeper investigation to enable it as a lead anticancer drug.

### 3.12. Apoptosis

To understand the mechanism of cell death, acridine orange/EB staining of HeLa cell was done. Acridine orange (AO) enters in all cells and makes the nuclei to appear green. If the cytoplasmic membrane integrity is lost then Ethidium bromide (EB) is taken up by cells and stains the nucleus red. EB also dominates over AO. Thus live cells have a normal green nucleus while early apoptotic cells have bright green nucleus with condensed or fragmented chromatin; late apoptotic cells having condensed and fragmented orange chromatin [61]. Untreated control cells having round and intact nucleus were stained green in Fig. 12. Control cell are live cell because integrity of cell membrane is maintained. In contrast, cells treated with ligand LH ( $65$   $\mu\text{M}$ ) show few early and late apoptotic cells because some cell are live stained green some cells have taken EB showing either completely stained orange cell (post apoptotic) or only nucleus is stained (apoptotic). Complex 1 ( $2$   $\mu\text{M}$ ) shows apoptosis only because all the cells are showing frag-mented nuclei stained orange. Complex 2 ( $25$   $\mu\text{M}$ ) show late apoptotic cell, because EB is taken by whole cell stained orange. Complex 1 is more effective than complex 2 because it is able to induce apoptosis in HeLa cell at lower concentration ( $2$   $\mu\text{M}$ ).

## 4. Conclusion

In summary, homo dinuclear complexes bearing Cu(II)-Cu(II) 1 and Zn(II)-Zn(II) 2 units, each bridged by nitrate group and embedded se-parately with a 2,2'-bipyridine and biologically relevant chalcone

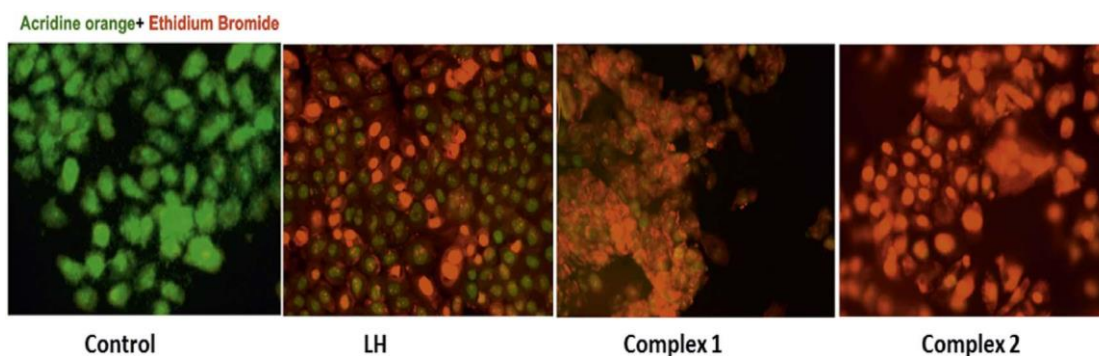


Fig. 12. HeLa cell lines showing staining of acridine orange (green) and EtBr (red) in both control condition as well as after treatment with drug LH ( $65$   $\mu\text{M}$ ), complex 1 ( $2$   $\mu\text{M}$ ) complex 2 ( $25$   $\mu\text{M}$ ). (For interpretation of the references to color in this figure legend, the reader is referred to the web version of this article.)

groups, are synthesized and characterized as penta-coordinated square pyramidal complexes bearing N<sub>2</sub>O<sub>3</sub> coordination core. Their solid state X-ray crystallography and ESR spectra (Cu(II) complex only) support their structures. Both complexes are arranged in anti-syn fashion. The structure and photophysical properties of the complexes are supported by their DFT and TD-DFT calculations. The redox property of copper (II) complex 1 has been studied using its cyclic voltammetry. In the process of investigation, biological activities of the complexes, the DNA cleavage capability of the complex, as well as DNA topoisomerase inhibition was studied which demonstrated their potential antitumor activity. The Cu (II) complex cleaves supercoiled DNA pBR322 significantly with its preferential binding to major groove of DNA and it follows oxidative pathway whereas Zn(II) complex follows hydrolytic cleavage pathway and prefers to bind with the minor groove of DNA. The complex 1 also inhibits catalytic activity of topoisomerase I with IC<sub>50</sub> value of 7 μM as compared to complex 2 with IC<sub>50</sub> value of 35 μM. Groove binding and topoisomerase I binding affinity with complexes 1 and 2 were also confirmed by molecular docking studies. The value to complex 1 is further added by the observation of its cytotoxicity with IC<sub>50</sub> value of 2.9 ± 0.021 μM against cervical cancer cell lines (HeLa cells). The complex 2 gave IC<sub>50</sub> value of 28.2 ± 0.044 μM. In the observed cytotoxicity of the two metal complexes, it is found that the metal ions play a significant role as two complexes of similar geometry differ only in metal ion. An early stage cell apoptosis induced by 1 makes it again interesting and enable it as a future candidate of anticancer drug.

#### Abbreviations

bpy	2,2'-bipyridine	
ESR	electron spin resonance	
MTT	3-(4,5-dimethylthiazol-2-yl)-2,5-diphenyltetrazolium bromide	
NC	nicked circular	
TD-DFT	Time Dependent Density Functional Theory	
DAPI	4',6-diamidino-2-phenylindole	
MG	methyl green	
EB	Ethidium bromide	
AO	Acridine orange	

#### Acknowledgements

Authors are thankful to authorities of CSIR grant no. 01 (2322)/09/ EMR-II and SERB grant no. SB/FT/CS-188/2013 New Delhi India for financial support.

#### Appendix A. Supplementary Data

Electronic supplementary information (ESI) available. CCDC reference no. 750137, 773965 and 858620 contains the supplementary crystallographic data for LH, complex 1 and 2 respectively. For ESI and crystallographic data in CIF or other electronic format ESI-MS the complexes 1 and 2, Time-dependent absorption spectral traces of complexes 1 and 2 recorded in 0–48 h, Time-dependent emission spectral traces of complexes 1 and 2 recorded in 0–48 h, the selected bond lengths (Å) and bond angles (°) for LH, complexes 1 and 2, Helical supramolecular structure of complex, Weak interaction parameter for the LH, 1 and 2, Supramolecular structure of complex 2, ESR Spectrum of complex 1, Cyclic voltammogram of complexes 1, Ethidium bromide stained agarose gel (1%) of pBR322 plasmid DNA (300 ng μL<sup>-1</sup>) in the presence of complex 1 and complex 2 (20 μM) with different activators after 1 h of incubation, Cytotoxicity profile of LH at different concentrations are available.

#### References

- [1] S. Komeda, A. Casini, *Curr. Top. Med. Chem.* 12 (2012) 219–235.
- [2] F. Mancin, P. Scrimin, P. Tecilla, U. Tonellato, *Chem. Commun.* (2005) 2540–2548.
- [3] X. Sheng, X. Guo, X.-M. Lu, G.-Y. Lu, Y. Shao, F. Liu, Q. Xu, *Bioconjug. Chem.* 19 (2008) 490–498.
- [4] R. Ott, R. Krämer, *Angew. Chem. Int. Ed.* 37 (1998) 1957–1960.
- [5] K. Jomova, M. Valko, *Toxicology* 283 (2011) 65–87.
- [6] L. Jia, J. Shi, Z.-h. Sun, F.-f. Li, Y. Wang, W.-N. Wu, Q. Wang, *Inorg. Chim. Acta* 391 (2012) 121–129.
- [7] V.M. Manikandamathavan, T. Weyhermüller, R.P. Parameswari, M. Sathishkumar, V. Subramanian, B.U. Nair, *Dalton Trans.* 43 (2014) 13018–13031.
- [8] T. Ito, S. Thyagarajan, K.D. Karlin, S.E. Rokita, *Chem. Commun.* (2005) 4812–4814.
- [9] W. Maret, *Metalloomics* 6 (2014) 1174.
- [10] W.E. Stehbins, *Exp. Mol. Pathol.* 75 (2003) 265–276.
- [11] K. Suntharalingam, A.J.P. White, R. Vilar, *Inorg. Chem.* 49 (2010) 8371–8380.
- [12] M.-G. Mendoza-Ferri, C.G. Hartinger, R.E. Eichinger, N. Stolyarova, K. Severin, M.A. Jakupec, A.A. Nazarov, B.K. Keppler, *Organometallics* 27 (2008) 2405–2407.
- [13] A. Medina-Molner, B. Spingler, *Chem. Commun.* 48 (2012) 1961–1963.
- [14] M.I. Khalil, A.M. AL-Zahem, M.M. Qunaibit, *Med. Chem. Res.* 23 (2014) 1683–1689.
- [15] C. Santini, M. Pellei, V. Gandin, M. Porchia, F. Tisato, C. Marzano, *Chem. Rev.* 114 (2014) 815–862.
- [16] Y.-J. Zhao, M.-C. Hong, Y.-C. Liang, W.-P. Su, R. Cao, Z.-Y. Zhou, A.S.C. Chan, *Polyhedron* 20 (2001) 2619–2625.
- [17] M.-C. Suen, G.-W. Tseng, J.-D. Chen, T.-C. Keng, J.-C. Wang, *Chem. Commun.* (1999) 1185–1186.
- [18] M.-Y. Chow, Z.Y. Zhou, T.C.W. Mak, *Inorg. Chem.* 31 (1992) 4900–4902.
- [19] Y.E. Filinchuk, V.V. Oliinik, V.N. Davydov, *Russ. J. Coord. Chem.* 23 (11) (1997) 791–793.
- [20] N. Dixit, R.K. Koiri, B.K. Maurya, S.K. Trigun, C. Höbartner, L. Mishra, *J. Inorg. Biochem.* 105 (2011) 256–267.
- [21] Y. Shi, B.B. Toms, N. Dixit, N. Kumari, L. Mishra, J. Goodisman, J.C. Dabrowiak, *Chem. Res. Toxicol.* 23 (2010) 1417–1426.
- [22] M.L. Go, X. Wu, X.L. Liu, *Curr. Med. Chem.* 12 (2005) 481–499.
- [23] R. Gaur, R.A. Khan, S. Tabassum, P. Shah, M.I. Siddiqi, L. Mishra, *J. Photochem. Photobiol. A Chem.* 220 (2011) 145–152.
- [24] R. Prajapati, S.K. Dubey, R. Gaur, R.K. Koiri, B.K. Maurya, S.K. Trigun, L. Mishra, *Polyhedron* 29 (2010) 1055–1061.
- [25] G.M. Sheldrick, *Acta Crystallogr. Sect. A* 64 (2008) 112–122.
- [26] I.J. Bruno, J.C. Cole, P.R. Edgington, M.K. Kessler, C.F. Macrae, P. McCabe, J. Pearson, R. Taylor, *Mercury*, *Acta Crystallogr. B* 58 (2002) 389.
- [27] A.L. Spek, *Platon*, *Acta Crystallogr. Sect. D* 65 (2009) 148–155.
- [28] S. Sen, S. Mitra, P. Kundu, M.K. Saha, C. Krüger, J. Bruckmann, *Polyhedron* 16 (1997) 2475–2481.
- [29] K.B. Raut, S.H. Wender, *J. Organomet. Chem.* 25 (1959) 50–52.
- [30] O. Trott, A.J. Olson, *J. Comput. Chem.* 31 (2010) 455–461.
- [31] M.F. Sanner, *J. Mol. Graphics Modell.* 17 (1999) 57–61.
- [32] Accelrys Software Inc, *Discovery Studio Modeling Environment*, Release 4.0, Accelrys Software Inc., San Diego, 2013.
- [33] The PyMOL Molecular Graphics System, Version 1.5.0.4, Schrödinger, LLC, 2013.
- [34] R. Gaur, L. Mishra, *RSC Adv.* 3 (2013) 12210–12219.
- [35] R. Gaur, L. Mishra, *Inorg. Chem.* 51 (2012) 3059–3070.
- [36] J. Tan, Y. Zhang, M. Zhang, X. Tian, Y. Wang, S. Li, C. Wang, H. Zhou, J. Yang, Y. Tian, J. Wu, *J. Mater. Chem. C* 4 (2016) 3256–3267.
- [37] U. Mukhopadhyay, I. Bernal, S.S. Massoud, F.A. Mautner, *Inorg. Chim. Acta* 357 (2004) 3673–3682.
- [38] K. Rurack, M.L. Dekhtyar, J.L. Bricks, U. Resch-Genger, W. Rettig, *J. Phys. Chem. A* 103 (1999) 9626–9635.
- [39] N. DiCesare, J.R. Lakowicz, *Tetrahedron Lett.* 43 (2002) 2615–2618.
- [40] T.A. Fayed, M.K. Awad, *Chem. Phys.* 303 (2004) 317–326.
- [41] E. Espada-Bellido, M.D. Galindo-Riño, M. García-Vargas, R. Narayanaswamy, *Appl. Spectrosc.* 64 (7) (2010) 727–732.
- [42] R. Prajapati, L. Mishra, S.J. Grabowski, G. Govil, S.K. Dubey, *J. Mol. Struct.* 879 (2008) 1–6.
- [43] J. Hausmann, M.H. Klingele, V. Lozan, G. Steinfeld, D. Siebert, Y. Jourmaux, J.J. Girerd, B. Kersting, *Chem. Eur. J.* 10 (2004) 1716–1728.
- [44] S.-K. Yoo, J.Y. Ryu, J.Y. Lee, C. Kim, S.-J. Kim, Y. Kim, *Dalton Trans.* (2003) 1454–1456.
- [45] A.W. Addison, T.N. Rao, J. Reedijk, J. Vanrijn, G.C. Verschoor, *J. Chem. Soc. Dalton Trans.* (1984) 1349–1356.
- [46] P. Roy, K. Dhara, M. Manassero, P. Banerjee, *Eur. J. Inorg. Chem.* (2008) 4404–4412.
- [47] V.K. Yadav, N. Kumari, L. Mishra, *Indian J. Chem., Sect. A* 50 (2011) 1035–1042.
- [48] R. Prajapati, L. Mishra, K. Kimura, P. Raghavaiah, *Polyhedron* 28 (2009) 600–608.
- [49] H.H. Monfareda, Z. Kalantaria, M.-A. Kamyabia, C. Janiak, *Z. Anorg. Allg. Chem.* 633 (2007) 1945–1948.
- [50] G. Palermo, A. Cavalli, M.L. Klein, M. Alfonso-Prieto, M.D. Peraro, M.D. Vivo, *Acc. Chem. Res.* 48 (2015) 220–228.
- [51] T. Jun, W. Bochua, Z. Liancai, *Bioorg. Med. Chem. Lett.* 17 (2007) 1197–1199.
- [52] H.-L. Seng, S.-T. Von, K.-W. Tan, M.J. Maah, S.-W. Ng, R.N. Rahman, I. Caracelli, C.-H. Ng, *Biometals* 23 (2010) 99–118.
- [53] M.R. Webb, S.E. Ebeler, *J. Food Biochem.* 32 (2008) 576–596.

- [54] M. Gupta, A. Fujimori, Y. Pommier, *Biochim. Biophys. Acta* 1262 (1995) 1–14.
- [55] S. Tabassum, W.M. Al-Asbahy, M. Afzal, F. Arjmand, V. Bagchi, *Dalton Trans.* 41 (2012) 4955–4964.
- [56] M.L. Rothenberg, *Ann. Oncol.* 8 (1997) 837–855.
- [57] S. Banerjee, S. Mondal, S. Sen, S. Das, D.L. Hughes, C. Rizzoli, C. Desplanches, C. Mandal, S. Mitra, *Dalton Trans.* (2009) 6849–6860.
- [58] N. Kumari, B.K. Maurya, R.K. Koiri, S.K. Trigun, S. Saripella, M.P. Coogan, L. Mishra, *Med. Chem. Commun.* 12 (2011) 1208–1216.
- [59] L. Jia, J. Xu, X. Zhao, S. Shen, T. Zhou, Z. Xu, T. Zhu, R. Chen, T. Ma, J. Xie, K. Dong, J.J. Huang, *Inorg. Biochem.* 159 (2016) 107–119.
- [60] A. Kosiha, C. Parthiban, K.P. Elango, *J. Photochem. Photobiol. B Biol.* 168 (2017) 165–174.
- [61] D. Ribble, N.B. Goldstein, D.A. Norris, Y.G. Shellman, *BMC Biotechnol.* (2005) 5–12.